

Measurement of Dijet Angular Distributions and Search for Quark Compositeness

- B. Abbott,²⁸ M. Abolins,²⁵ B. S. Acharya,⁴³ I. Adam,¹² D. L. Adams,³⁷ M. Adams,¹⁷ S. Ahn,¹⁴ H. Aihara,²²
 G. A. Alves,¹⁰ E. Amidi,²⁹ N. Amos,²⁴ E. W. Anderson,¹⁹ R. Astur,⁴² M. M. Baarmand,⁴² A. Baden,²³ V. Balamurali,³²
 J. Balderston,¹⁶ B. Baldin,¹⁴ S. Banerjee,⁴³ J. Bantly,⁵ J. F. Bartlett,¹⁴ K. Bazizi,³⁹ A. Belyaev,²⁶ S. B. Beri,³⁴
 I. Bertram,³¹ V. A. Bezzubov,³⁵ P. C. Bhat,¹⁴ V. Bhatnagar,³⁴ M. Bhattacharjee,¹³ N. Biswas,³² G. Blazey,³⁰
 S. Blessing,¹⁵ P. Bloom,⁷ A. Boehlein,¹⁴ N. I. Bojko,³⁵ F. Borcherding,¹⁴ C. Boswell,⁹ A. Brandt,¹⁴ R. Brock,²⁵
 A. Bross,¹⁴ D. Buchholz,³¹ V. S. Burtovoi,³⁵ J. M. Butler,³ W. Carvalho,¹⁰ D. Casey,³⁹ Z. Casilum,⁴²
 H. Castilla-Valdez,¹¹ D. Chakraborty,⁴² S.-M. Chang,²⁹ S. V. Chekulaev,³⁵ L.-P. Chen,²² W. Chen,⁴² S. Choi,⁴¹
 S. Chopra,²⁴ B. C. Choudhary,⁹ J. H. Christenson,¹⁴ M. Chung,¹⁷ D. Claes,²⁷ A. R. Clark,²² W. G. Cobau,²³ J. Cochran,⁹
 W. E. Cooper,¹⁴ C. Cretsinger,³⁹ D. Cullen-Vidal,⁵ M. A. C. Cummings,¹⁶ D. Cutts,⁵ O. I. Dahl,²² K. Davis,² K. De,⁴⁴
 K. Del Signore,²⁴ M. Demarteau,¹⁴ D. Denisov,¹⁴ S. P. Denisov,³⁵ H. T. Diehl,¹⁴ M. Diesburg,¹⁴ G. Di Loreto,²⁵
 P. Draper,⁴⁴ Y. Ducros,⁴⁰ L. V. Dudko,²⁶ S. R. Dugad,⁴³ D. Edmunds,²⁵ J. Ellison,⁹ V. D. Elvira,⁴² R. Engelmann,⁴²
 S. Eno,²³ G. Eppley,³⁷ P. Ermolov,²⁶ O. V. Eroshin,³⁵ V. N. Evdokimov,³⁵ T. Fahland,⁸ M. Fatya,⁴ M. K. Fatya,³⁹
 J. Featherly,⁴ S. Feher,¹⁴ D. Fein,² T. Ferbel,³⁹ G. Finocchiaro,⁴² H. E. Fisk,¹⁴ Y. Fisyak,⁷ E. Flattum,¹⁴ G. E. Forden,²
 M. Fortner,³⁰ K. C. Frame,²⁵ S. Fuess,¹⁴ E. Gallas,⁴⁴ A. N. Galyaev,³⁵ P. Gartung,⁹ T. L. Geld,²⁵ R. J. Genik II,²⁵
 K. Genser,¹⁴ C. E. Gerber,¹⁴ B. Gibbard,⁴ S. Glenn,⁷ B. Gobbi,³¹ M. Goforth,¹⁵ A. Goldschmidt,²² B. Gómez,¹
 G. Gómez,²³ P. I. Goncharov,³⁵ J. L. González Solís,¹¹ H. Gordon,⁴ L. T. Goss,⁴⁵ K. Gounder,⁹ A. Goussiou,⁴²
 N. Graf,⁴ P. D. Grannis,⁴² D. R. Green,¹⁴ J. Green,³⁰ H. Greenlee,¹⁴ G. Grim,⁷ S. Grinstein,⁶ N. Grossman,¹⁴
 P. Grudberg,²² S. Grünendahl,³⁹ G. Guglielmo,³³ J. A. Guida,² J. M. Guida,⁵ A. Gupta,⁴³ S. N. Gurzhiev,³⁵
 P. Gutierrez,³³ Y. E. Gutnikov,³⁵ N. J. Hadley,²³ H. Haggerty,¹⁴ S. Hagopian,¹⁵ V. Hagopian,¹⁵ K. S. Hahn,³⁹
 R. E. Hall,⁸ P. Hanlet,²⁹ S. Hansen,¹⁴ J. M. Hauptman,¹⁹ D. Hedin,³⁰ A. P. Heinson,³⁰ U. Heintz,¹⁴
 R. Hernández-Montoya,¹¹ T. Heuring,¹⁵ R. Hirosky,¹⁵ J. D. Hobbs,¹⁴ B. Hoeneisen,^{1,*} J. S. Hoftun,⁵ F. Hsieh,²⁴
 Ting Hu,⁴² Tong Hu,¹⁸ T. Huehn,⁹ A. S. Ito,¹⁴ E. James,² J. Jaques,³² S. A. Jerger,²⁵ R. Jesik,¹⁸ J. Z.-Y. Jiang,⁴²
 T. Joffe-Minor,³¹ K. Johns,² M. Johnson,¹⁴ A. Jonckheere,¹⁴ M. Jones,¹⁶ H. Jöstlein,¹⁴ S. Y. Jun,³¹ C. K. Jung,⁴²
 S. Kahn,⁴ G. Kalbfleisch,³³ J. S. Kang,²⁰ R. Kehoe,³² M. L. Kelly,³² C. L. Kim,²⁰ S. K. Kim,⁴¹ A. Klatchko,¹⁵
 B. Klima,¹⁴ C. Klopfenstein,⁷ V. I. Klyukhin,³⁵ V. I. Kochetkov,³⁵ J. M. Kohli,³⁴ D. Koltick,³⁶ A. V. Kostritskiy,³⁵
 J. Kotcher,⁴ A. V. Kotwal,¹² J. Kourlas,²⁸ A. V. Kozelov,³⁵ E. A. Kozlovski,³⁵ J. Krane,²⁷ M. R. Kirshnaswamy,⁴³
 S. Krzywdzinski,¹⁴ S. Kunori,²³ S. Lami,⁴² H. Lan,^{14,†} R. Lander,⁷ F. Landry,²⁵ G. Landsberg,¹⁴ B. Lauer,¹⁹
 A. Leflat,²⁶ H. Li,⁴² J. Li,⁴⁴ Q. Z. Li-Demarteau,¹⁴ J. G. R. Lima,³⁸ D. Lincoln,²⁴ S. L. Linn,¹⁵ J. Linnemann,²⁵
 R. Lipton,¹⁴ Q. Liu,^{14,†} Y. C. Liu,³¹ F. Lobkowicz,³⁹ S. C. Loken,²² S. Lökö,⁴² L. Lueking,¹⁴ A. L. Lyon,²³
 A. K. A. Maciel,¹⁰ R. J. Madaras,²² R. Madden,¹⁵ L. Magaña-Mendoza,¹¹ S. Mani,⁷ H. S. Mao,^{14,†} R. Markeloff,³⁰
 T. Marshall,¹⁸ M. I. Martin,¹⁴ K. M. Mauritz,¹⁹ B. May,³¹ A. A. Mayorov,³⁵ R. McCarthy,⁴² J. McDonald,¹⁵
 T. McKibben,¹⁷ J. McKinley,²⁵ T. McMahon,³³ H. L. Melanson,¹⁴ M. Merkin,²⁶ K. W. Merritt,¹⁴ H. Miettinen,³⁷
 A. Mincer,²⁸ C. S. Mishra,¹⁴ N. Mokhov,¹⁴ N. K. Mondal,⁴³ H. E. Montgomery,¹⁴ P. Mooney,¹ H. da Motta,¹⁰
 C. Murphy,¹⁷ F. Nang,² M. Narain,¹⁴ V. S. Narasimham,⁴³ A. Narayanan,² H. A. Neal,²⁴ J. P. Negret,¹ P. Nemethy,²⁸
 M. Nicola,¹⁰ D. Norman,⁴⁵ L. Oesch,²⁴ V. Oguri,³⁸ E. Oltman,²² N. Oshima,¹⁴ D. Owen,²⁵ P. Padley,³⁷ M. Pang,¹⁹
 A. Para,¹⁴ Y. M. Park,²¹ R. Partridge,⁵ N. Parua,⁴³ M. Paterno,³⁹ J. Perkins,⁴⁴ M. Peters,¹⁶ R. Piegaia,⁶ H. Piekarz,¹⁵
 Y. Pischanikov,³⁶ V. M. Podstavkov,³⁵ B. G. Pope,²⁵ H. B. Prosper,¹⁵ S. Protopopescu,⁴ J. Qian,²⁴ P. Z. Quintas,¹⁴
 R. Raja,¹⁴ S. Rajagopalan,⁴ O. Ramirez,¹⁷ L. Rasmussen,⁴² S. Reucroft,²⁹ M. Rijssenbeek,⁴² T. Rockwell,²⁵
 N. A. Roe,²² P. Rubinov,³¹ R. Ruchti,³² J. Rutherford,² A. Sánchez-Hernández,¹¹ A. Santoro,¹⁰ L. Sawyer,⁴⁴
 R. D. Schamberger,⁴² H. Schellman,³¹ J. Sculli,²⁸ E. Shabalina,²⁶ C. Shaffer,¹⁵ H. C. Shankar,⁴³ R. K. Shivpuri,¹³
 M. Shupe,² H. Singh,⁹ J. B. Singh,³⁴ V. Sirotenko,³⁰ W. Smart,¹⁴ R. P. Smith,¹⁴ R. Snihur,³¹ G. R. Snow,²⁷ J. Snow,³³
 S. Snyder,⁴ J. Solomon,¹⁷ P. M. Sood,³⁴ M. Sosebee,⁴⁴ N. Sotnikova,²⁶ M. Souza,¹⁰ A. L. Spadafora,²²
 R. W. Stephens,⁴⁴ M. L. Stevenson,²² D. Stewart,²⁴ F. Stichelbaut,⁴² D. A. Stoianova,³⁵ D. Stoker,⁸ M. Strauss,³³
 K. Streets,²⁸ M. Strovink,²² A. Sznajder,¹⁰ P. Tamburello,²³ J. Tarazi,⁸ M. Tartaglia,¹⁴ T. L. T. Thomas,³¹
 J. Thompson,²³ T. G. Trippe,²² P. M. Tuts,¹² N. Varelas,²⁵ E. W. Varnes,²² D. Vititoe,² A. A. Volkov,³⁵
 A. P. Vorobiev,³⁵ H. D. Wahl,¹⁵ G. Wang,¹⁵ J. Warchol,³² G. Watts,⁵ M. Wayne,³² H. Weerts,²⁵ A. White,⁴⁴
 J. T. White,⁴⁵ J. A. Wightman,¹⁹ S. Willis,³⁰ S. J. Wimpenny,⁹ J. V. D. Wirjawan,⁴⁵ J. Womersley,¹⁴ E. Won,³⁹

D. R. Wood,²⁹ H. Xu,⁵ R. Yamada,¹⁴ P. Yamin,⁴ C. Yanagisawa,⁴² J. Yang,²⁸ T. Yasuda,²⁹ P. Yepes,³⁷ C. Yoshikawa,¹⁶ S. Youssef,¹⁵ J. Yu,¹⁴ Y. Yu,⁴¹ Z. H. Zhu,³⁹ D. Ziemska,¹⁸ A. Ziemsinski,¹⁸ E. G. Zverev,²⁶ and A. Zylberstein⁴⁰

(D0 Collaboration)

¹Universidad de los Andes, Bogotá, Colombia

²University of Arizona, Tucson, Arizona 85721

³Boston University, Boston, Massachusetts 02215

⁴Brookhaven National Laboratory, Upton, New York 11973

⁵Brown University, Providence, Rhode Island 02912

⁶Universidad de Buenos Aires, Buenos Aires, Argentina

⁷University of California, Davis, California 95616

⁸University of California, Irvine, California 92697

⁹University of California, Riverside, California 92521

¹⁰LAFEX, Centro Brasileiro de Pesquisas Físicas, Rio de Janeiro, Brazil

¹¹CINVESTAV, Mexico City, Mexico

¹²Columbia University, New York, New York 10027

¹³Delhi University, Delhi, India 110007

¹⁴Fermi National Accelerator Laboratory, Batavia, Illinois 60510

¹⁵Florida State University, Tallahassee, Florida 32306

¹⁶University of Hawaii, Honolulu, Hawaii 96822

¹⁷University of Illinois at Chicago, Chicago, Illinois 60607

¹⁸Indiana University, Bloomington, Indiana 47405

¹⁹Iowa State University, Ames, Iowa 50011

²⁰Korea University, Seoul, Korea

²¹Kyungsung University, Pusan, Korea

²²Lawrence Berkeley National Laboratory and University of California, Berkeley, California 94720

²³University of Maryland, College Park, Maryland 20742

²⁴University of Michigan, Ann Arbor, Michigan 48109

²⁵Michigan State University, East Lansing, Michigan 48824

²⁶Moscow State University, Moscow, Russia

²⁷University of Nebraska, Lincoln, Nebraska 68588

²⁸New York University, New York, New York 10003

²⁹Northeastern University, Boston, Massachusetts 02115

³⁰Northern Illinois University, DeKalb, Illinois 60115

³¹Northwestern University, Evanston, Illinois 60208

³²University of Notre Dame, Notre Dame, Indiana 46556

³³University of Oklahoma, Norman, Oklahoma 73019

³⁴University of Panjab, Chandigarh 16-00-14, India

³⁵Institute for High Energy Physics, 142-284 Protvino, Russia

³⁶Purdue University, West Lafayette, Indiana 47907

³⁷Rice University, Houston, Texas 77005

³⁸Universidade do Estado do Rio de Janeiro, Brazil

³⁹University of Rochester, Rochester, New York 14627

⁴⁰CEA, DAPNIA/Service de Physique des Particules, CE-SACLAY, Gif-sur-Yvette, France

⁴¹Seoul National University, Seoul, Korea

⁴²State University of New York, Stony Brook, New York 11794

⁴³Tata Institute of Fundamental Research, Colaba, Mumbai 400005, India

⁴⁴University of Texas, Arlington, Texas 76019

⁴⁵Texas A&M University, College Station, Texas 77843

(Received 7 July 1997)

We have measured the dijet angular distribution in $\sqrt{s} = 1.8$ TeV $p\bar{p}$ collisions using the D0 detector. Order α_s^3 QCD predictions are in good agreement with the data. At 95% confidence limit the data exclude models of quark compositeness in which the contact interaction scale is below 2 TeV. [S0031-9007(97)05129-6]

PACS numbers: 13.87.Ce, 12.38.Qk, 12.60.Rc, 13.85.Ni

In this Letter we present a new measurement of the angular distribution of dijets produced in $p\bar{p}$ collisions over a wide angular range and at higher precision than previous measurements [1]. In quantum chromodynamics (QCD), parton-parton scattering processes are mainly

t -channel exchanges and produce dijet angular distributions peaked at small center-of-mass (CM) scattering angles; many processes containing new physics are more isotropic. Dijet final states in $p\bar{p}$ collisions can be produced through quark-quark, quark-gluon, and gluon-gluon

interactions. The angular distributions produced by these processes as predicted by theory are similar. Therefore the dijet angular distribution is insensitive to the relative weighting of the individual hard scattering process and thus is insulated from uncertainties in the parton distribution functions (pdf's). Thus, the dijet angular distribution provides an excellent test of QCD and a means of searching for new physics such as quark compositeness. Next-to-leading order (NLO) QCD predictions are available [2,3] and comparisons can be made between the data and both leading order (LO) and NLO predictions.

The value of the mass scale, Λ , characterizes the strength of the quark substructure binding interactions and the physical size of the composite states. In the regime where $\Lambda \gg \sqrt{s}$ is valid, the quarks appear almost pointlike and any quark substructure coupling can be approximated by a four-Fermi interaction. With this approximation, the effective Lagrangian for a flavor diagonal definite chirality current is [4,5]: $\mathcal{L} = A(2\pi/\Lambda^2) \times (\bar{q}_H \gamma^\mu q_H)(\bar{q}_H \gamma_\mu q_H)$ where $A = \pm 1$, and $H = L, R$ for left- or right-handed quarks. While this is not the only possible contact interaction, it is the only one for which calculations are currently available. Since the sign of A is *a priori* undetermined, limits for constructive interference ($A = -1$) and destructive interference ($A = +1$) are presented. Recently published results from CDF [1] on dijet angular distributions have been compared to the same model in which all quarks are composite, yielding 95% confidence limits $\Lambda^+ > 1.8$ TeV and $\Lambda^- > 1.6$ TeV on the interaction scales.

The D0 detector, described in detail elsewhere [6], measures jets using uranium, liquid-argon sampling calorimeters that provide uniform and hermetic coverage over a large range of pseudorapidity ($|\eta| \leq 4$). Typical transverse segmentation is 0.1×0.1 in $\eta \times \phi$, where ϕ is the azimuthal angle.

The data are from the 94 pb^{-1} sample recorded during the 1993–1995 Tevatron run. Events are selected using a multilevel trigger. The first level requires an inelastic collision by demanding the coincidence of two hodoscopes on either side of the interaction region. In the second level, jet candidates are selected using an array of 40 calorimeter trigger towers 0.8×1.6 in $\eta \times \phi$, covering $|\eta| < 4$. Four different trigger criteria are defined, each requiring a single trigger tower above a different transverse energy (E_T) threshold. The final level, an online software trigger, selects events with a jet above a preset threshold. The E_T thresholds at which the triggers are $>98\%$ efficient for the η coverage used in this analysis are 55, 90, 120, and 175 GeV.

Jets are reconstructed using a fixed cone algorithm with radius $\mathcal{R} = \sqrt{\Delta\eta^2 + \Delta\phi^2} = 0.7$. Calorimeter towers with E_T greater than 1.0 GeV are used as seed towers for jet finding [7]. Jet E_T is defined as the sum of the E_T in the towers with $\mathcal{R} < 0.7$ from the seed tower and a new E_T weighted center of the jet is calculated. This process is repeated until the jet center is stable. When

one jet overlaps another, they are merged into a single jet if they share more than 50% of the E_T of the lower E_T jet. Otherwise, they are split into two distinct jets.

Jet energy calibration is performed in a multistep process [8]. First, the electromagnetic energy scale in the central calorimeter is determined by scaling the energies of electrons from Z boson decays so that the corrected Z mass agrees with the value measured at LEP [9]. Next, the jet response of the central calorimeter is measured using momentum conservation in a sample of photon + jet events. After determining the jet response for the central calorimeter as a function of jet energy, the relative η dependent jet response is measured using both photon + jet and dijet events. One jet (photon) is required to be central, and the jet response is measured as a function of the η of the other jet. Jets are also corrected for out-of-cone showering losses, underlying event, multiple $p\bar{p}$ interactions, and effects of uranium noise.

Quality cuts are required for the two leading E_T jets in each event. These cuts eliminate spurious jets that arise from noisy calorimeter cells, cosmic rays, and accelerator losses. The efficiencies for these cuts are E_T and η dependent and vary between 90% and 97%.

We define the mean $\eta_{\text{boost}} = \frac{1}{2}(\eta_1 + \eta_2)$ and the half difference $\eta^* = \frac{1}{2}(\eta_1 - \eta_2)$ of the pseudorapidities of the two jets with highest E_T . Data are selected in bands of dijet invariant mass M , where $M^2 = 2E_{T1}E_{T2}[\cosh 2\eta^* - \cos(\phi_1 - \phi_2)]$, neglecting the jet masses. To maintain uniform acceptance [10], we require $|\eta_{1,2}| < 3$ and $|\eta_{\text{boost}}| < 1.5$.

The dominant spin-1 gluon exchange yields a distribution in the CM scattering angle $\theta^* = \cos^{-1}(\tanh \eta^*)$ similar to Rutherford scattering: $dN_{\text{Ruth}}/d\cos \theta^* \propto 1/\sin^4(\theta^*/2)$. We transform θ^* to $\chi = e^{2|\eta^*|} = (1 + |\cos \theta^*|)/(1 - |\cos \theta^*|)$, so that large θ^* maps to small χ (e.g., $\theta^* = 90^\circ \leftrightarrow \chi = 1$). Then $dN_{\text{Ruth}}/d\chi$ is independent of χ , facilitating a comparison with theory.

Table I shows the dijet angular distribution, $(100/N)(dN/d\chi)$, in bins of $\Delta\chi = 1$ with its statistical error in the four mass bins. The JETRAD program [3] is used to determine the LO and NLO QCD predictions. The jets at NLO are found using the standard [11] jet definition which combines two partons into a single jet if they are both within $\mathcal{R} = 0.7$ of their E_T weighted center. We require that two partons also be closer than $\mathcal{R}_{\text{sep}} \times 0.7$ with $\mathcal{R}_{\text{sep}} = 1.3$ [12,13]. Figure 1 shows the dijet angular distributions normalized to the unit area compared to three different theoretical predictions. The dashed and solid curves show the LO and NLO predictions for a single choice of renormalization/factorization scale, $\mu = E_T$ of the maximum E_T jet. The dotted curve shows the effects of changing the scale to $\mu = E_T^{\max}/2$ for the NLO predictions. The LO predictions are fairly insensitive to the renormalization scale, so only one scale is shown. With the large value of χ_{\max} , the effects of higher order QCD become apparent. The theoretical predictions are clearly sensitive to the order of the calculation

TABLE I. Dijet angular distribution ($100/N$) ($dN/d\chi$) with statistical uncertainties for the four mass bins (GeV/c^2).

χ	$260 < M < 425$	$425 < M < 475$	$475 < M < 635$	$M > 635$
1.5	5.94 ± 0.36	7.58 ± 0.69	10.1 ± 0.34	12.0 ± 1.04
2.5	5.50 ± 0.35	4.26 ± 0.52	7.56 ± 0.30	12.5 ± 1.06
3.5	4.59 ± 0.32	4.96 ± 0.57	7.83 ± 0.30	9.11 ± 0.91
4.5	4.57 ± 0.32	5.54 ± 0.59	7.71 ± 0.30	9.79 ± 0.95
5.5	4.56 ± 0.32	5.29 ± 0.58	7.87 ± 0.31	10.1 ± 0.97
6.5	5.10 ± 0.33	6.26 ± 0.64	8.17 ± 0.31	9.58 ± 0.95
7.5	5.10 ± 0.33	4.83 ± 0.56	8.70 ± 0.32	9.30 ± 0.94
8.5	5.61 ± 0.35	4.40 ± 0.53	7.91 ± 0.31	8.08 ± 0.88
9.5	4.93 ± 0.33	5.60 ± 0.60	8.46 ± 0.32	8.96 ± 0.92
10.5	6.04 ± 0.36	5.21 ± 0.58	8.62 ± 0.32	10.6 ± 1.01
11.5	5.40 ± 0.34	4.30 ± 0.53	8.38 ± 0.32	
12.5	5.33 ± 0.34	4.75 ± 0.55	8.69 ± 0.32	
13.5	5.41 ± 0.34	5.43 ± 0.58		
14.5	5.40 ± 0.34	5.69 ± 0.60		
15.5	5.60 ± 0.35	6.18 ± 0.63		
16.5	4.81 ± 0.32	4.70 ± 0.55		
17.5	4.95 ± 0.33	4.83 ± 0.55		
18.5	5.78 ± 0.35	5.01 ± 0.56		
19.5	5.37 ± 0.34	5.17 ± 0.57		

and to the renormalization scale. The NLO predictions are seen to be in better agreement with the data than the LO calculations, especially for large χ .

The dominant source of error on the angular distribution is the uncertainty in the η dependence of the calorimeter energy scale. This uncertainty is less than 4% and nearly independent of dijet invariant mass. The remaining sys-

tematic uncertainty is due to η biases in jet reconstruction, multiple $p\bar{p}$ interactions, η dependent jet quality cut efficiencies, and effects of calorimeter η and E_T smearing. Because the data distributions are normalized to the unit area, uncertainties in the absolute jet energy scale are minimal. All systematic uncertainties added in quadrature are shown as a band at the bottom of Fig. 1. The effects of a different pdf were examined by replacing the default CTEQ3M [14] with CTEQ2MS [15]. The calculated angular distribution is insensitive to this change.

Because the currently available NLO calculations do not implement the effects of both QCD and quark substructure, possible effects of quark compositeness are determined using a LO simulation [4]. The ratio of the LO predictions with compositeness to the LO predictions with no compositeness is used to scale the NLO calculations. Figure 2 shows the dijet angular distribution for events with $M > 635 \text{ GeV}/c^2$ compared to the theory for different values of the compositeness scale, Λ^+ . The largest dijet invariant mass bin is shown because the effects of quark compositeness become more pronounced with increasing dijet invariant mass.

To obtain a compositeness limit, we constructed the variable R_χ , the ratio of the number of events with $\chi < 4$ to the number of events with $4 < \chi < \chi_{\max}$. The value $\chi = 4$ is chosen to optimize the sensitivity to quark compositeness. Because the angular distribution of jets arising from contact interactions is expected to be more isotropic than that for QCD interactions, contact interactions will produce more events at small χ than QCD and therefore will have a larger value of R_χ . The η dependent energy scale corrections increase as a function of invariant mass causing R_χ to be reduced by 8% in the lowest mass bin and by 28% in the highest mass bin. Table II shows the

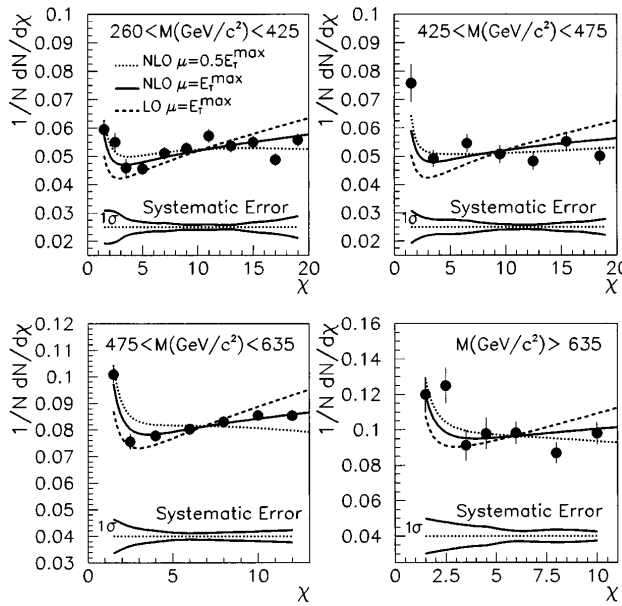


FIG. 1. Dijet angular distributions for D0 data (points) compared to JETRAD for LO (dashed line) and NLO predictions with renormalization/factorization scale $\mu = E_T^{\max}$ (solid line). The data are also compared to JETRAD NLO predictions with $\mu = E_T^{\max}/2$ (dotted line). The errors on the data points are statistical only. The band at the bottom represents the correlated $\pm 1\sigma$ systematic uncertainty.

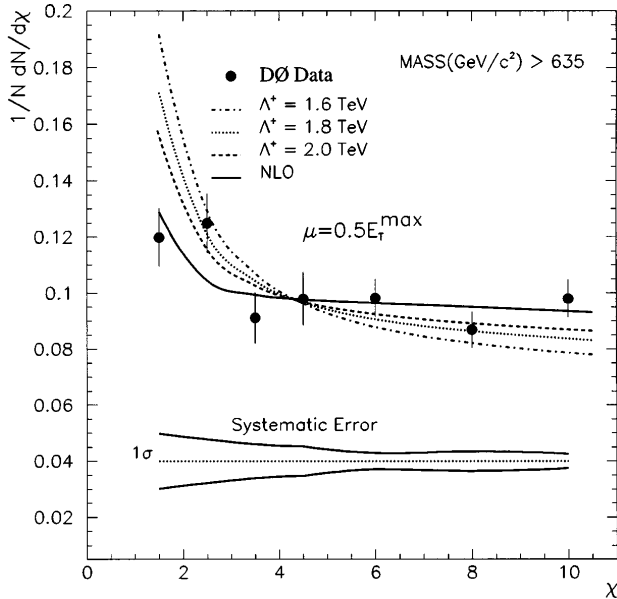


FIG. 2. Data compared to theory for different compositeness scales. See text for how compositeness is calculated for NLO predictions. The errors on the points are statistical and the band represents the correlated $\pm 1\sigma$ systematic uncertainty.

experimental ratio R_χ for the different mass ranges with their statistical and their systematic uncertainties, which are fully correlated in mass. Figure 3 exhibits R_χ as a function of M for two different renormalization scales along with the theoretical predictions for different compositeness scales. Note that the two largest dijet invariant mass bins have a lower χ_{\max} value, and thus a higher value of R_χ is expected independent of compositeness assumptions. Also shown in Fig. 3 are the χ^2 values for the 4 degrees of freedom for different values of the compositeness scale. The χ^2 is defined as $\chi^2 = \sum_{i,j} \delta_i V_{ij}^{-1} \delta_j$, where δ_i is the difference between data and theory in each mass bin i . The covariance matrix, V , is defined as $V_{ii} = \sigma_i^2(\text{stat}) + \sigma_i^2(\text{syst})$, $V_{ij} = \sigma_i(\text{syst})\sigma_j(\text{syst})$, for $i \neq j$. For both renormalization scales, the data prefer a model without quark compositeness. The data are better fit with $\mu = E_T^{\max}$.

We employed a Bayesian technique [16] to obtain a compositeness scale limit from our data, using a Gaussian likelihood function, $P(R_\chi | \xi)$, for R_χ as a function of dijet invariant mass. The compositeness limit depends on the choice of the prior probability distribution, $P(\xi)$. Motivated by the form of the Lagrangian, $P(\xi)$ is as-

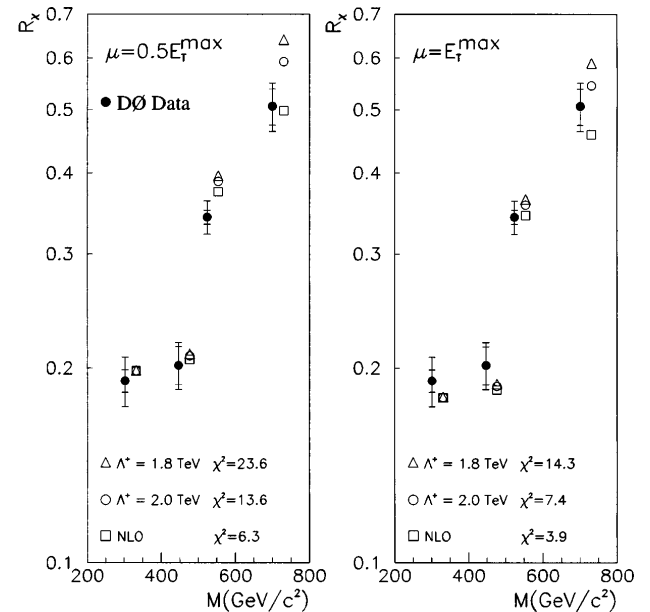


FIG. 3. R_χ as a function of dijet invariant mass for two different renormalization scales. See text for how compositeness is calculated for NLO predictions. The inner error bars are the statistical uncertainties and the outer error bars include the statistical and systematic uncertainties added in quadrature. The χ^2 values for the 4 degrees of freedom are shown for the different values of the compositeness scale. The D0 data are plotted at the average mass for each mass range. The NLO points are offset in mass to allow the data points to be seen.

sumed to be flat either in $\xi = 1/\Lambda^2$ or $\xi = 1/\Lambda^4$. Since the dijet angular distribution at NLO is sensitive to the renormalization scale, each renormalization scale is treated as a different theory. The likelihood function has the form $P(R_\chi | \xi) = e^{-\chi^2/2}$. To determine the 95% confidence limit in Λ , a limit in ξ is first calculated by requiring that $Q(\xi) = \int_0^\xi P(R_\chi | \xi') P(\xi') d\xi' = 0.95$ of $Q(\infty)$. The limit in ξ is then transformed back into a limit in Λ . Table III shows the 95% confidence limits for the compositeness scale obtained for different choices of models using a prior probability distribution which is flat in $1/\Lambda^2$.

If we vary the models to include constructive interference (Λ^-), or require only up and down quarks to be composite (Λ_{ud}), the 95% confidence limits for the compositeness scale change by ~ 0.1 TeV. If the prior probability distribution is assumed to be flat in $1/\Lambda^4$, the 95% confidence limits are reduced by approximately 6%. These limits are valid for either pure left- or right-handed

TABLE II. Value of R_χ with statistical and fully correlated systematic uncertainties.

Mass range (GeV/c ²)	R_χ	Stat error	Syst error
260–425	0.191	0.0077	0.015
425–475	0.202	0.0136	0.010
475–635	0.342	0.0085	0.018
>635	0.506	0.0324	0.028

TABLE III. The 95% confidence limits for the left-handed contact compositeness scale for different models. The prior probability distribution is assumed to be flat in $1/\Lambda^2$.

Compositeness scale	$\mu = E_T^{\max}$	$\mu = E_T^{\max}/2$
Λ^+	2.1 TeV	2.3 TeV
Λ^-	2.2 TeV	2.4 TeV
Λ_{ud}^+	1.9 TeV	2.0 TeV
Λ_{ud}^-	2.0 TeV	2.2 TeV

contact interactions. Unlike the earlier measurement [1] using $\chi_{\max} = 5$, the large range of χ explored here gives greater sensitivity to compositeness terms with constructive interference than for destructive interference.

In conclusion, we have measured the dijet angular distribution over a large angular range. The data distributions are in good agreement with NLO QCD predictions. The compositeness limit depends on the choice of the renormalization/factorization scale, the model of compositeness, and the choice of the prior probability function. We have presented compositeness limits for models with left-handed contact interference. With 95% confidence, the interaction scales $\Lambda^{+(-)}$ exceed 2.1 TeV and $\Lambda_{ud}^{+(-)}$ exceed 1.9 TeV.

We thank R. Harris for the use of his program based on Ref. [5]. We also thank the staffs at Fermilab and collaborating institutions for their contributions to this work, and acknowledge support from the Department of Energy and National Science Foundation (U.S.A.), Commissariat à L'Energie Atomique (France), State Committee for Science and Technology and Ministry for Atomic Energy (Russia), CNPq (Brazil), Departments of Atomic Energy and Science and Education (India), Colciencias (Colombia), CONACyT (Mexico), Ministry of Education and KOSEF (Korea), and CONICET and UBACyt (Argentina).

*Visitor from Univ. San Francisco de Quito, Ecuador.

[†]Visitor from IHEP, Beijing, China.

[1] CDF Collaboration, F. Abe *et al.*, Phys. Rev. Lett. **62**,

- 3020 (1989); CDF Collaboration, F. Abe *et al.*, Phys. Rev. Lett. **69**, 2896 (1992); CDF Collaboration, F. Abe *et al.*, Phys. Rev. Lett. **77**, 5336 (1996); **78**, 4307(E) (1997).
[2] S. D. Ellis, Z. Kunszt, and D. E. Soper, Phys. Rev. Lett. **64**, 2121 (1990).
[3] W. T. Giele, E. W. N. Glover, and D. A. Kosower, Nucl. Phys. **B403**, 633 (1993).
[4] E. Eichten, K. Lane, and M. Peskin, Phys. Rev. Lett. **50**, 811 (1983).
[5] K. Lane, Report No. BUHEP-96-8, hep-ph/9605257, 1996.
[6] D0 Collaboration, S. Abachi *et al.*, Nucl. Instrum. Methods Phys. Res., Sect. A **338**, 185 (1994).
[7] D0 Collaboration, S. Abachi *et al.*, Phys. Lett. B **357**, 500 (1995).
[8] B. Abbott *et al.*, Report No. Fermilab-Pub-97/330-E, (http://www-d0.fnal.gov/d0pubs/energy_scale/jet_energy_scale.html) (to be published).
[9] Particle Data Group, L. Montanet *et al.*, “Review of Particle Properties,” Phys. Rev. D **50**, 1336 (1994).
[10] Mary K. Fatyga, Ph.D. dissertation, University of Rochester, 1996 (unpublished).
[11] J. Huth *et al.*, in *Proceedings of Research Directions for the Decade, Snowmass 1990*, edited by E. L. Berger (World Scientific, Singapore, 1992).
[12] S. D. Ellis, Z. Kunszt, and D. E. Soper, Phys. Rev. Lett. **69**, 3615 (1992).
[13] B. Abbott *et al.*, Report No. Fermilab-Pub-97/242-E.
[14] CTEQ Collaboration, H. L. Lai *et al.*, Phys. Rev. D **51**, 4763 (1995).
[15] CTEQ Collaboration, J. Botts *et al.*, Phys. Lett. B **304**, 159 (1993).
[16] H. Jeffreys, *Theory of Probability* (Clarendon Press, Oxford, 1939), p. 94.